

ARTICLE OPEN



Tracing genomic instability in induced mesenchymal stromal cell manufacture: an integration-free transfection approach

Jong-Mi Lee^{1,2,7}, Chae Yeon Lee^{1,3,7}, Binna Seol^{4,7}, Chan Kwon Jung⁵, Yonggoo Kim^{1,2}, Dain Kang¹, Haein Yu¹, Yuna Hong^{1,3}, Cho Lok Song⁴, Yee Sook Cho^{4,6}✉ and Myungshin Kim^{1,3}✉

© The Author(s) 2025

Here we systematically investigated genomic alterations from the initiation of induced pluripotent stem (iPS) cell generation to induced mesenchymal stromal/stem cell differentiation. We observed a total of ten copy number alterations (CNAs) and five single-nucleotide variations (SNVs) during the phases of reprogramming, differentiation and passaging. We identified a higher frequency of CNAs and SNVs in iPS cells generated using the Sendai virus (SV) method compared with those generated with episomal vectors (Epi). Specifically, all SV-iPS cell lines exhibited CNAs during the reprogramming phase, while only 40% of Epi-iPS cells showed such alterations. Additionally, SNVs were observed exclusively in SV-derived cells during passaging and differentiation, with no SNVs detected in Epi-derived lines. Gene expression analysis revealed upregulation of chromosomal instability-related genes in late-passage SV-iPSCs, further indicating increased genomic instability. Notably, *TP53* mutations were identified, underscoring the vulnerability of the gene and the critical need for careful genomic scrutiny when preparing iPS cells and derived cell lines.

Experimental & Molecular Medicine (2025) 57:900–909; <https://doi.org/10.1038/s12276-025-01439-8>

INTRODUCTION

Mesenchymal stromal/stem (MS) cells are a population of non-hematopoietic adherent cells derived from bone marrow, adipose tissue or placental tissue. They can differentiate into various types of tissues, such as bone, cartilage and adipose tissue¹. MS cells have great potential for clinical applications, particularly in tissue repair and regeneration². Recently, there has been a growing interest in generating functional MS cells from induced pluripotent stem (iPS) cells as a potential source of high-quality cells for regenerative medicine^{3,4}.

iPS cell-derived MS cells (iMS cells) have been successfully generated and exhibit phenotypes and biological functions similar to MS cells. iMS cells are more homogeneous and predictable than primary MS cells, as they originate from a single iPS cell clone and their molecular signature remains stable among different batches⁵. iPS cells can provide stable and reliable sources of iMS cells, greatly expanding the clinical applications of iMS cells for treating various diseases, such as cardiovascular diseases and bone and cartilage disorders^{3,5}.

Notably, iPS cells can experience genomic instability at any stage of their generation, and mutations may arise during differentiation to final cell products. This is a potential concern when using iMS cells for therapeutic applications⁶. Through replication, MS cells accumulate genomic instability, represented by abundant single-nucleotide variations (SNVs) and copy number alterations (CNAs) at late passages^{7,8}.

Therefore, this study aimed to investigate the genomic changes occurring during the process of generating and passaging iPS cells and differentiating them into iMS cells, as well as the changes that occur during iMS cell passage. We utilized a range of techniques, including chromosome analysis, chromosomal microarray, short tandem duplication and next-generation sequencing (NGS), to comprehensively evaluate the genomic changes that occurred throughout the entire process. By defining the genomic scenarios occurring during iMS cell generation, differentiation and passaging, we hope to gain insights into the safety and efficacy of using iMS cells in regenerative medicine.

MATERIALS AND METHODS

Ethics

All studies involving human and animal experiments were approved by the Institutional Review Board (P01-201910-31-005), the Institutional Animal Care and Use Committee of the Korea Research Institute of Bioscience and Biotechnology (KRIBB) (KRIBB-AEC-19153) and the Institutional Review Board of Seoul St. Mary's Hospital (KC18BNSI0110).

Generation of iPS cells from fibroblasts and characterization

Cell culture. Human skin fibroblasts (CRL-2097, American Type Culture Collection) were cultured in fibroblast medium containing 85% minimum essential medium-α (α-MEM, Thermo Fisher Scientific), supplemented with 15% FBS, 1% penicillin/streptomycin, 1× MEM non-essential amino acids (NEAAs) and 1% sodium pyruvate (all from Thermo Fisher Scientific).

¹Catholic Genetic Laboratory Center, Seoul St. Mary's Hospital, College of Medicine, The Catholic University of Korea, Seoul, Republic of Korea. ²Department of Laboratory Medicine, College of Medicine, The Catholic University of Korea, Seoul, Republic of Korea. ³Department of Medical Sciences, Graduate School of The Catholic University of Korea, Seoul, Republic of Korea. ⁴Stem Cell Research Laboratory, Immunotherapy Research Center, Korea Research Institute of Bioscience and Biotechnology (KRIBB), Daejeon, Republic of Korea. ⁵Department of Hospital Pathology, College of Medicine, The Catholic University of Korea, Seoul, Republic of Korea. ⁶Department of Bioscience, KRIBB School, University of Science and Technology, Daejeon, Republic of Korea. ⁷These authors contributed equally: Jong-Mi Lee, Chae Yeon Lee, Binna Seol. ✉email: june@kribb.re.kr; microkim@catholic.ac.kr

Received: 22 December 2023 Revised: 6 December 2024 Accepted: 2 February 2025

Published online: 14 April 2025

Primary umbilical cord-derived mesenchymal stem cells (UC-MS cells, human; PCS-500-010) were obtained from American Type Culture Collection.

Derivation of iPS cells. To establish the integration-free iPS cell lines, we reprogrammed human skin fibroblasts into iPS cells using Sendai virus vectors (CytoTune-iPS 2.0 Sendai Reprogramming kit (Thermo Fisher Scientific) encoding Oct4, Sox2, Klf4 and c-Myc or non-viral episomal plasmid vectors (Episomal iPS cell reprogramming vectors, Thermo Fisher Scientific) encoding Oct4, Sox2, Klf4, l-Myc, Lin28A and shp53 based on a previous protocol with a slight modification⁹. To generate Sendai virus vector-based iPS cells (SV-iPS cells), human fibroblasts were counted and plated at a density of 1×10^5 cells in a six-well plate. After 2 days, cells were transduced with SVs in fibroblast medium with 4 µg/ml of polybrene (Sigma) and incubated overnight at 37 °C in a CO₂ incubator. The following day, the medium was replaced with fresh medium and incubated for 4 days, with the medium changed every other day. From day 6 onward, the medium was changed to iPS cell medium (mTeSR1; StemCell Technologies) and replaced daily until iPS cell colonies appeared. To generate episomal vector-based iPS cells (Epi-iPS cells), human fibroblasts (1×10^6 cells per reaction) were electroporated with episomal vectors using the Neon Transfection System (Thermo Fisher Scientific). The electroporated cells were plated in a well of a six-well plate and incubated for 5 days in fibroblast medium, with the medium changed every other day. Cells were plated at a density of $1\text{--}5 \times 10^4$ cells per well in a six-well plate. The following day, the medium was replaced with iPS cell medium mTeSR1 every day until iPS cell colonies appeared. iPS cell colonies were manually selected, transferred to 12-well plates and expanded in mTeSR1 with daily changes for additional analysis. The iPS cell colonies were manually passaged every 5–7 days throughout the experiments.

ALP staining. Alkaline phosphatase (ALP) staining was performed for 30 min at room temperature using the Vector Red Alkaline Phosphatase Substrate kit I (Sigma) according to the manufacturer's instructions. Images were captured using a microscope (IX51; Olympus).

Immunocytochemistry staining. For immunocytochemical staining, iPS cells were fixed in 4% formaldehyde in phosphate-buffered saline (PBS) for 15 min and permeabilized with 0.1% Triton X-100 in PBS for 30 min at room temperature. After blocking with 4% bovine serum albumin for 2 h, the fixed cells were incubated with primary antibodies overnight at 4 °C. The following primary antibodies were used: Oct3/4 (H-134) (1:100, sc-9081, Santa Cruz), Nanog (1:40, AF1997, R&D Systems), Tra-1-81 (1:100, MAB4381, Millipore), SSEA-3 (1:30, MAB1434, R&D Systems), Tra-1-60 (1:100, MAB4360, Millipore), SSEA-4 (1:30, MAB1435, R&D Systems), Tuj1 (1:500, 802001, Biolegend), Nestin (1:100, MAB5326, Millipore), Desmin (1:50, AB907, Millipore), Actin, alpha-Smooth Muscle (α-SMA) (1:200, A5228, Sigma), HNF3beta/FOXA2 (1:100, 07-633, Millipore), SOX17 (1:50, MAB1924, R&D Systems) and phospho-Histone H2A.X (Ser139), clone JBW301 (1:500, 05-636, Millipore). Primary antibodies were detected using Alexa Fluor 594 and 488 (1:200; Thermo Fisher Scientific) conjugated with secondary antibodies. Nuclei were stained with 4,6-diamidino-2-phenylindole (DAPI). All fluorescence images were acquired using an Axio VertA.1 microscope (Carl Zeiss) and a LSM 800 Laser Scanning Confocal Microscope (Carl Zeiss). The antibodies used in this study are listed in Supplementary Table 1.

Three-germ layer differentiation of iPS cells. To validate the spontaneous three-germ layer differentiation potential of iPS cells, in vitro differentiation was induced by the formation of embryonic bodies (EBs), as previously described⁹. For EB formation, clumps of iPS cells were cultured in EB medium consisting of knockout DMEM supplemented with 10% KSR, 1% NEAA, 0.1 mM β-mercaptoethanol and 1 mM L-glutamine for 5 days on Petri dishes. The medium was changed every other day. Floating EBs were seeded on gelatin-coated plates and cultured for an additional 10 days. The medium was changed every other day.

Teratoma formation. For teratoma formation, iPS cells (2×10^6 cells) were prepared in 50 µl of PBS/Matrigel (BD Biosciences) and injected subcutaneously into the dorsal flank of 4-week-old CAnN.Cg-Foxn1 nu/CrljOri mice (ORIENT Bio. Inc.). Ten weeks after injection, the teratomas were collected, dissected and fixed in 4% formaldehyde. The teratoma tissues were then processed, embedded in paraffin wax and sectioned at 5 µm. Sectioned teratomas were analyzed using hematoxylin and eosin staining.

Mycoplasma test. The absence of mycoplasma contamination was assessed via PCR using the EZ-PCR Mycoplasma detection kit (Biological Industries).

Differentiation of iPS cells into iMS cells

Differentiation into iMS cells. SV-iPS cells and Epi-iPS cells were differentiated into MS cells (SV-iMS cells and Epi-iMS cells, respectively) using the STEMdiff Mesenchymal Progenitor kit (StemCell Technologies) according to the manufacturer's instructions. SV-iPS cells and Epi-iPS cells were plated at a density of 5×10^4 cells/cm² on six-well plates precoated with Matrigel and cultured in mTeSR1 for 2 days with daily medium changes. After washing with Dulbecco's phosphate-buffered saline (DPBS), iPS cells were cultured with STEMdiff-ACF mesenchymal induction medium for 4 days, with daily medium changes. After washing with DPBS (Thermo Fisher Scientific), iPS cells were cultured with MesenCult-ACF medium for 2 days with daily medium changes and then passaged into six-well plates precoated with MesenCult-ACF Attachment Substrate. Cells were subcultured with 0.25% (w/v) trypsin–EDTA until they reached approximately 70–80% confluency. The medium was changed daily for 15 days. Finally, differentiated iMS cells were cultured and expanded at a density of 1×10^4 cells/cm² in MesenCult-ACF Medium or MS cell medium containing 90% α-MEM, supplemented with 10% FBS, 1% penicillin/streptomycin, 1× MEM NEAA, 1× GlutaMAX and 5 ng/ml basic fibroblast growth factor (R&D Systems).

Flow cytometry. Single-cell dissociated SV-iMS cells and Epi-iMS cells were stained with PE-conjugated CD73, PE-conjugated CD105, PE-conjugated CD90 (Miltenyi Biotec); CD34/CD45 Cocktail, FITC, PE (Thermo Fisher Scientific); FITC-conjugated HLA-ABC and FITC-conjugated HLA-DR (BioLegend) for 30 min and protected from light. The stained cells were washed twice with PBS. Flow cytometric analysis was performed using a BD Accuri C6 flow cytometer (BD Biosciences) to detect the cell surface markers of SV-iMS cells and Epi-iMS cells. The antibodies used in this study are listed in Supplementary Table 1.

Tri-lineage differentiation of iMS cells. Tri-lineage differentiation of iMS cells was performed using an Osteogenesis, Adipogenesis and Chondrogenesis Differentiation kit (Thermo Fisher Scientific), according to the manufacturer's protocol. iMS cells were seeded at a density of 5000 cells/cm² in 24-well plates and incubated in the MS cell medium. The next day, the cells were transferred to osteogenic, adipogenic and chondrogenic differentiation medium and incubated until differentiation was complete. Fresh differentiation medium was changed every 3 days. After differentiation, Alizarin Red, Oil Red O and Alcian blue dyes (Sigma) were used to visualize the presence of calcified matrix, lipid droplets and cartilage matrix, respectively. Briefly, after fixing the differentiated cells with 4% formaldehyde for 10 min, the cells were washed three times with distilled water and stained with Alizarin Red (2%), Oil Red O (0.5%) and Alcian Blue solution (1%) at room temperature.

Assessment of tumorigenicity of iMS cells. To study the tumorigenic properties of iMS cells, we used ten NSG mice (NOD scid gamma mice; NOD.Cg-Prkdc^{scid}Il2rg^{tm1Wjl}/SzJ, Jackson Laboratory), comprising five females and five males, all 7 weeks old. Each mouse was injected subcutaneously with a cell suspension of 1.0×10^7 iMS cells combined with Matrigel (BD Biosciences) in a volume of 200 µl. We monitored the iMS cell implantation site for morphological changes for up to 12 months and meticulously recorded our observations. At the end of the observation period, we performed thorough necropsies on each animal. The retrieved tissues were immediately fixed in formalin and prepared for detailed pathological examination.

RT-qPCR

Total RNA was isolated using the RNeasy Mini kit (Qiagen) according to the manufacturer's protocol. RNA (2 µg) was reverse transcribed using a SuperScript VILO cDNA Synthesis Kit (Thermo Fisher Scientific). Quantitative PCR with reverse transcription (RT-qPCR) was performed using the SYBR Green Real-time PCR Master Mix (Roche Diagnostics GmbH) on a 7500 Fast Real-Time PCR System (Applied Biosystems). The expression of tissue-specific genes were measured and normalized to that of the housekeeping gene *GAPDH*. The primers used are listed in Supplementary Table 2.

Evaluation of genomic stability

Karyotyping. Chromosomal analyses of iPS cell lines were performed according to a previously described method¹⁰. Briefly, cultured cells were treated by colcemid. Cells were collected using trypsin and treated by prewarmed hypotonic KCl solution. After fixation with a 1:3 acetic acid:methanol solution, slides were prepared for chromosomal analysis using the trypsin–Giemsa banding technique. At least 20 metaphase samples were analyzed.

STR analysis. Genomic DNA was extracted using the Wizard Genomic DNA Purification kit (Promega) and used for further genomic stability analyses, including short tandem repeat (STR) analysis. STR analysis was performed using AmpFISTR Identifier PCR amplification to confirm iPS cell line identity (Applied Biosystems), according to the method used in previous study¹¹.

Chromosomal microarray. CNAs were analyzed using SurePrint G3 Human CGH+SNP microarray 4× 180K kit (Agilent Technologies) and/or the Affymetrix CytoScan Dx Assay kit (Affymetrix), according to the manufacturers' recommended methods used in our previous studies⁸. Identified CNAs were validated using an alternative platform (either SurePrint or Affymetrix, as applicable). Genomic Workbench 7.0.4.0 software (Agilent Technologies) and Chromosome Analysis Suite Dx (ChAS Dx) v1.3 Affymetrix Software package were used to determine CNAs.

NGS. We used the OncoPrint Comprehensive Panel v3M (Thermo Fisher Scientific), and OncoPrint Childhood Cancer Research Assay kit (Thermo Fisher Scientific) according to the manufacturer's instruction¹². Sequencing was performed on an Ion S5 XL Sequencer (Thermo Fisher Scientific) and analyzed using the Ion Torrent Server software (Thermo Fisher Scientific). Detected mutations were validated using the TruSight Oncology 500 assay (Illumina). DNA libraries were prepared, enriched, and sequenced on NextSeq 550 Dx (Illumina). Sequencing data were analyzed using the TruSight Oncology 500 Local App Version 2.2 (Illumina). Elaborate sequence data in FASTQ format were adjusted and annotated according to the hg19 human reference genome. The variant allele fraction was calculated by dividing the number of mutant sequencing reads by the total number of reads. All detected mutations were verified manually using Integrative Genomic Viewer¹⁹.

RNA sequencing

To evaluate gene expression changes between reprogramming methods, total RNA sequencing was performed on representative cells (SV-iPS cell and Epi-iPS cell) at both mid- and late passages. Libraries were prepared using the Illumina Stranded Total RNA Prep with Ribo-Zero Plus (Illumina) with 800 ng of total RNA, followed by sequencing on an Illumina NovaSeq-6000 sequencer (Illumina). The sequencing data were analyzed using the CLC Genomics Workbench 20.0.4 (Qiagen). The FASTQ files were processed and annotated using the hg38 human reference genome. Gene expression quantification was normalized to transcripts per million, and fold changes in differentially expression genes (DEGs) were calculated.

The chromosomal instability 25 (CIN25) gene signature, which includes specific genes whose expression is consistently correlated with total functional aneuploidy¹³, was evaluated by calculating the log₂ fold change in expression levels. Statistical significance for each DEG was determined using a *P* value of <0.05. To further explore the impact of passaging on gene expression, we conducted Gene Set Enrichment Analysis (GSEA) to identify changes in DEGs. A false discovery rate *q* value of <0.05 and family-wise error rate *P* value of <0.05 was considered statistically significant.

Statistical analysis

The data are presented as the means ± s.d. of at least three separate experiments. Comparisons between two groups were analyzed using Student's *t*-tests. Significance was established at **P* < 0.05 and ***P* < 0.01. All analyses were performed using SPSS for Windows (version 24.0; IBM Corp.).

RESULTS

Characterization of integration-free iPS cells

We generated four independent SV-iPS cells and five Epi-iPS cells for use in this study (Fig. 1a). Fully reprogrammed iPS cell lines

exhibited typical human embryonic stem cell-like morphology (Fig. 1b). Pluripotency was confirmed by classical assays. Immunocytochemical analysis showed strong expression of the transcription factors Oct3/4 and Nanog, as well as the surface markers SSEA-3, SSEA-4, TRA-1-60 and TRA-1-81 in undifferentiated SV-iPS cells and Epi-iPS cells (Fig. 1b). In addition, the analysis of in vitro differentiation potential of SV-iPS cells and Epi-iPS cells indicated their contribution to all three germ layers (ecto-, meso- and endoderm) (Fig. 1c and Supplementary Fig. 2c). The potential of SV-iPS cells and Epi-iPS cells to differentiate into the three germ layers was further verified in vivo using teratoma assays (Fig. 1d). STR analysis confirmed the genetic identity of all SV-iPS cell and Epi-iPS cell lines with the parental cells (Supplementary Fig. 1a). SV-iPS cells and Epi-iPS cells retained their normal karyotype for over 60 passages (Fig. 1e) without mycoplasma contamination (Supplementary Fig. 1b). The pluripotency of SV-iPS cells and Epi-iPS cells used for the genomic stability and tumorigenicity studies was confirmed by the presence of pluripotency markers (Supplementary Fig. 2a,b).

Characterization of iMS cells

SV-iPS cells and Epi-iPS cells reprogrammed from human fibroblasts were subjected to mesenchymal differentiation to produce iMS cells for 21 days in a commercial MS cell differentiation medium (Fig. 2a). Our results revealed that both SV-iMS cells and Epi-iMS cells exhibited a typical fibroblast-like morphology (Fig. 2b). During passage, the cells constituted a homogeneous population of fibroblasts (Fig. 2b). The expression of MS cell-specific cell surface markers in passaged iMS cells was evaluated using flow cytometry. Flow cytometric analysis showed that SV-iMS cell 1 (at p5 and p10) and Epi-iMS cell 1 (at p5 and p10) were negative for antigens CD34, CD45 and HLA-DR and positive for known antigens of MS cells, CD73, CD90, CD105 and HLA-ABC^{14–17}. Less than 5% of the analyzed cell population expressed CD34 or CD45 at any passage. The expression levels of CD73, CD105, CD90 and HLA-ABC were stable and high throughout all passages (Fig. 2c). We observed that MS cell-specific surface marker properties were preserved after passaging for p15–17, as confirmed via RT-qPCR analysis (Supplementary Fig. 3a). MS cell characteristics of SV-iMS cells and Epi-iMS cells used for genomic stability and tumorigenicity studies were confirmed by the presence of MS cell-specific markers and/or absence of pluripotency marker (Supplementary Fig. 3b). The typical MS cell-like properties of SV-iMS cells and Epi-iMS cells were assessed based on their multilineage differentiation potential into osteoblasts, chondrocytes and adipocytes. In osteogenic differentiation, both SV-iMS cells and Epi-iMS cells formed extracellular calcium matrices, as demonstrated by Alizarin Red S staining (Fig. 3a). Chondrogenic differentiation was confirmed by the accumulation of sulfated proteoglycans, visualized by Alcian blue staining (Fig. 3a). For adipogenic differentiation, the accumulation of lipid droplets within the cells was observed through Oil Red O staining (Fig. 3a). Real-time PCR analysis further supported these findings by detecting the expression of lineage-specific markers: alkaline phosphatase (*ALP*), osteocalcin (*OCN*) and collagen type I (*COL1A1*) for osteoblasts; *SOX9*, collagen type II (*COL2A1*) and aggrecan (*ACAN*) for chondrocytes; and perilipin1 (*PLIN1*), lipoprotein lipase (*LPL*) and peroxisome proliferator-activated receptor-gamma (*PPARγ2*) for adipocytes (Fig. 3b). No substantial differences were observed in the differentiation capacity between SV-iMS cells, Epi-iMS cells and control UC-MS cells, indicating comparable lineage-specific differentiation potential across all groups.

The in vivo tumorigenicity assay demonstrated that all NSG mice survived for 12 months after receiving an injection of an iMS cell suspension. Throughout the observation period, no tumors were detected at the injection sites. Additionally, tissue specimens taken from the injection sites showed no microscopic pathological abnormalities.

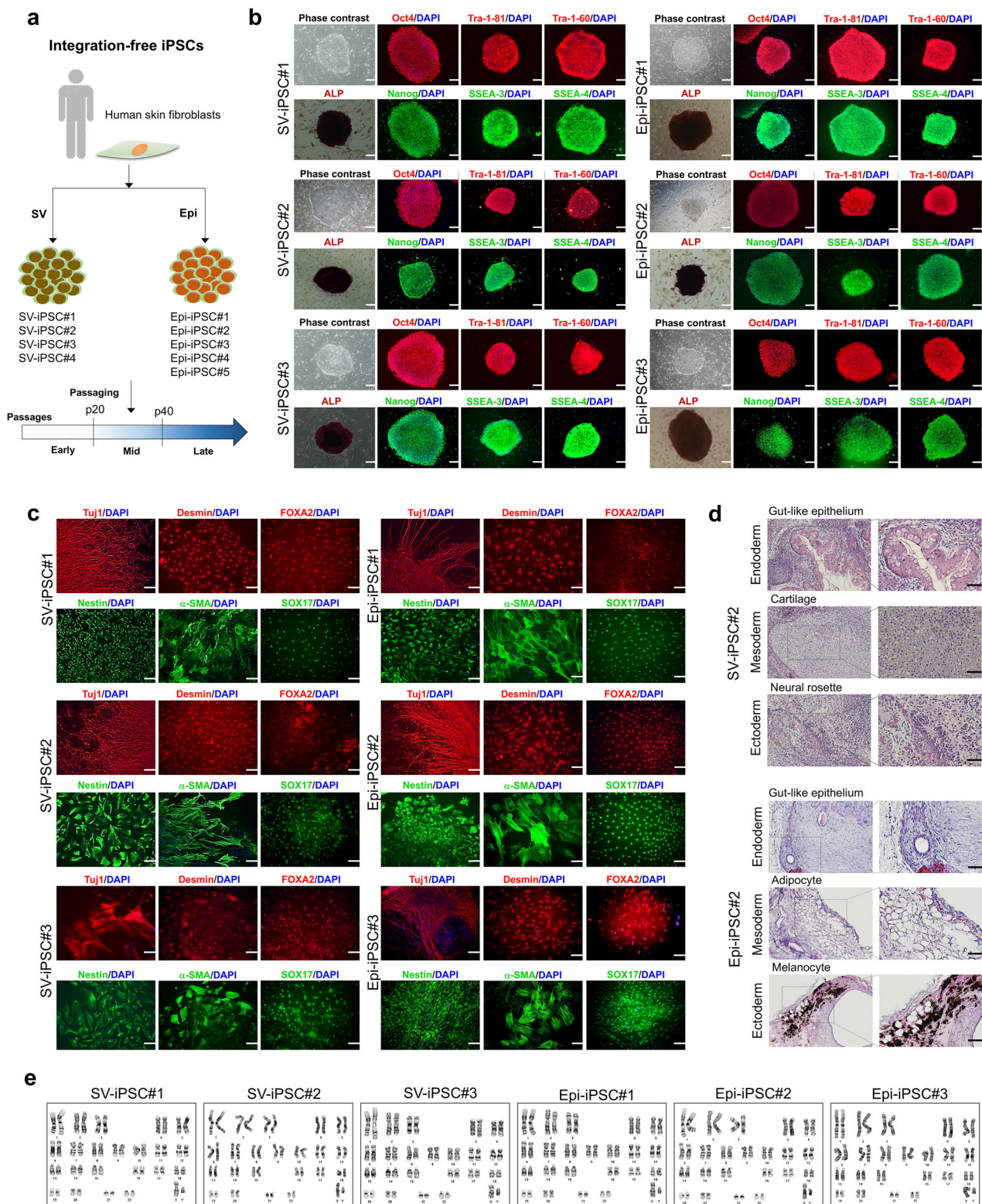


Fig. 1 Generation and characterization of iPSC cells. **a**, An overview of integration-free iPSC cell generation. Pluripotency characterization was performed using passages 7–10. **b**, Immunocytochemistry analysis of pluripotency markers (Oct4, Nanog, Tra-1-81, Tra-1-60, SSEA-3 and SSEA-4) and ALP staining in iPSC cells generated using SV (SV-iPSC cell) and episomal vectors (Epi-iPSC cell). Nuclei were stained by DAPI. Scale bar, 200 μ m. **c**, Immunocytochemistry analysis of markers for the three-germ layers (Tuj1 and Nestin (ectoderm); FOXA2 and SOX17 (endoderm); Desmin and α -SMA (mesoderm)) in in vitro differentiated SV-iPSC cells and Epi-iPSC cells. Scale bar, 100 μ m. **d**, Hematoxylin and eosin staining of teratomas generated with SV-iPSC cells and Epi-iPSC cells. Differentiation into multiple derivatives of three-germ layers is shown: ectoderm (melanocyte, neural rosette), endoderm (gut-like epithelium) and mesoderm (adipocyte, cartilage). Scale bar, 50 μ m. **e**, Normal karyotype of Epi-iPSC cells and SV-iPSC cells.

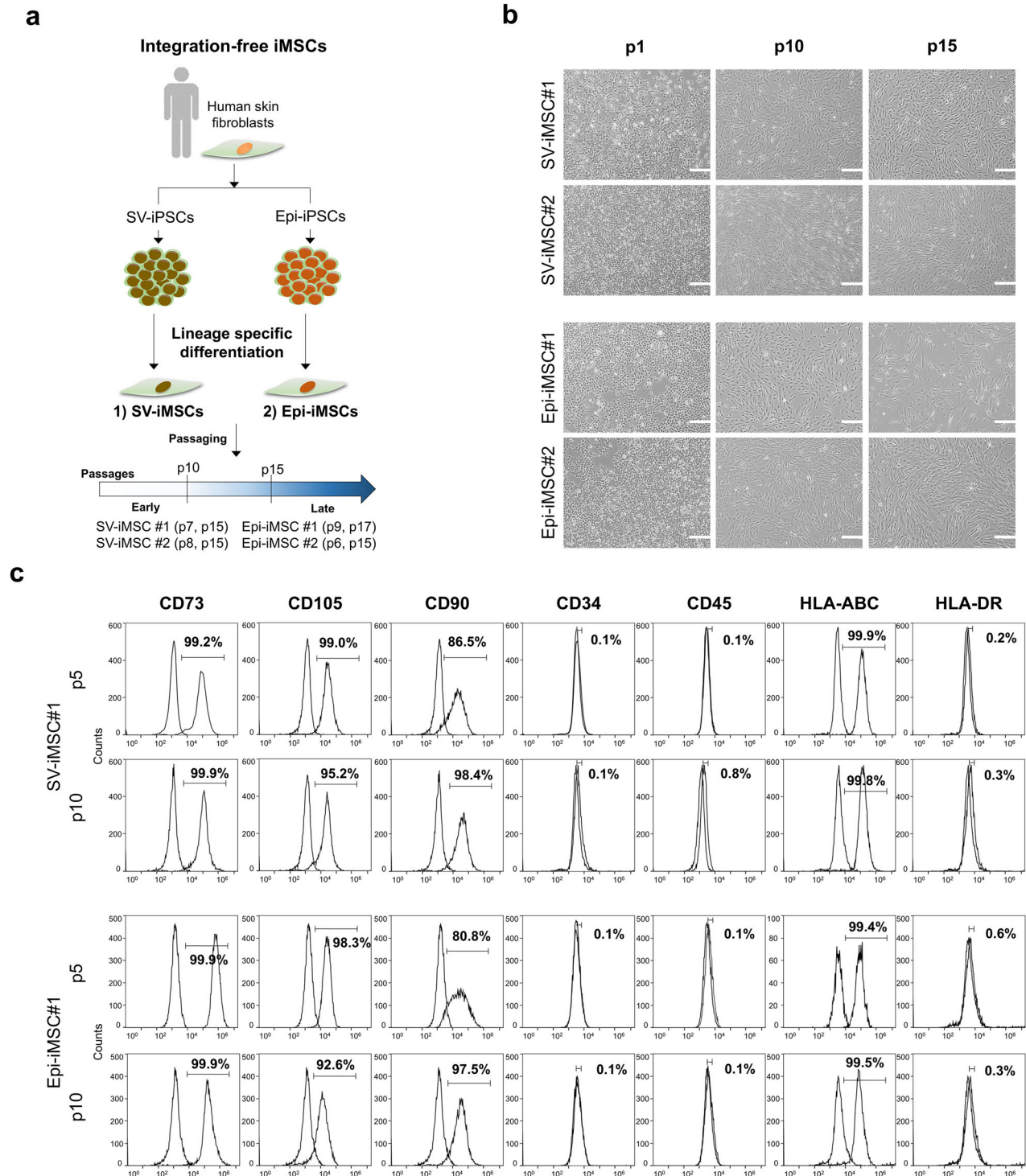


Fig. 2 Generation and characterization of iMS cells. **a**, An overview of integration-free iMS cell generation. MS cell characterization was performed using passages 4–6. **b**, Phase-contrast images of iMS cells generated using SV (SV-iMS cell) and episomal vectors (Epi-iMS cell). Scale bar, 200 μ m. **c**, Flow cytometric analysis of MS cell markers (CD73, CD105 and CD90), hematopoietic markers (CD34 and CD45), HLA class I (HLA-ABC) and HLA class II (HLA-DR) in passaged SV-iMS cell 1 (at p5 and p10) and Epi-iMS cell 1 (at p5 and p10).

Replication stress and DNA damage

Elevated levels of phosphorylation of histone H2AX on serine 139 (γ H2AX) in iPSCs indicate replication stress and DNA damage, both of which are crucial to monitor for genomic stability¹⁸. We examined and compared the level of γ H2AX in the human skin fibroblasts (p6 versus p30), SV-iPSCs (p11 versus p41), Epi-iPSCs (p35 versus p42), SV-iMS cells (p7 versus p15) and Epi-iMS

cells (p9 versus p17). In a control experiment, a significant increase in γ H2AX foci staining was observed when the fibroblasts (p6) were treated with doxorubicin and aphidicolin, known inducers of replication stress (Supplementary Fig. 4a,b). Both SV-iPSCs and Epi-iPSCs exhibited higher basal levels of γ H2AX compared with fibroblasts and iMS cells, indicating greater replication stress and DNA damage. As expected, replication stress was more

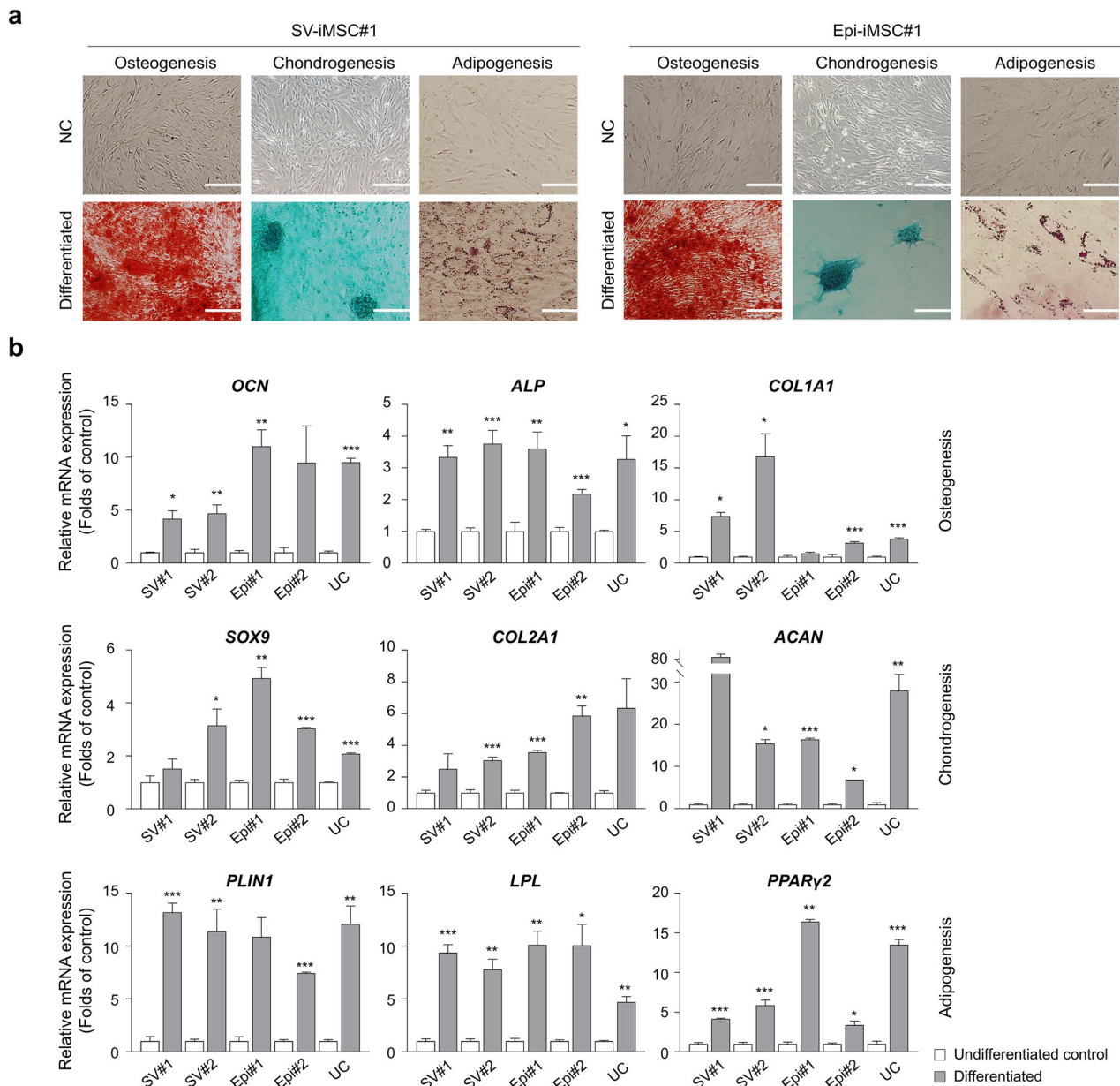


Fig. 3 Differentiation potential of iMS cells using two integration-free methods: SV-iPS cells and Epi-iPS cell into osteoblasts, chondrocytes and adipocytes *in vitro*. **a**, Representative staining of osteoblasts (Alizarin red staining, left, scale bar, 200 μ m), chondrocytes (Alcian blue staining, middle, scale bar, 100 μ m), adipocytes (Oil red O staining, right, scale bar, 50 μ m) and negative control (NC) groups. **b**, Relative expression levels of lineage-specific markers measured by RT-qPCR: *OCN*, *ALP* and *COL1A1* for osteoblasts; *SOX9*, *COL2A1* and *ACAN* for chondrocytes; and *PLIN1*, *LPL* and *PPARγ2* for adipocytes. The UC-MS cells were verified as the control primary MS cells. Data represent means \pm s.d. of three independent experiments. * P < 0.05, ** P < 0.01 and *** P < 0.001 compared with undifferentiated control (t-test). SV#1, SV-iMS cell 1; SV#2, SV-iMS cell 2; Epi#1, Epi-iMS cell 1; Epi#2, Epi-iMS cell 2; UC, UC-MS cell.

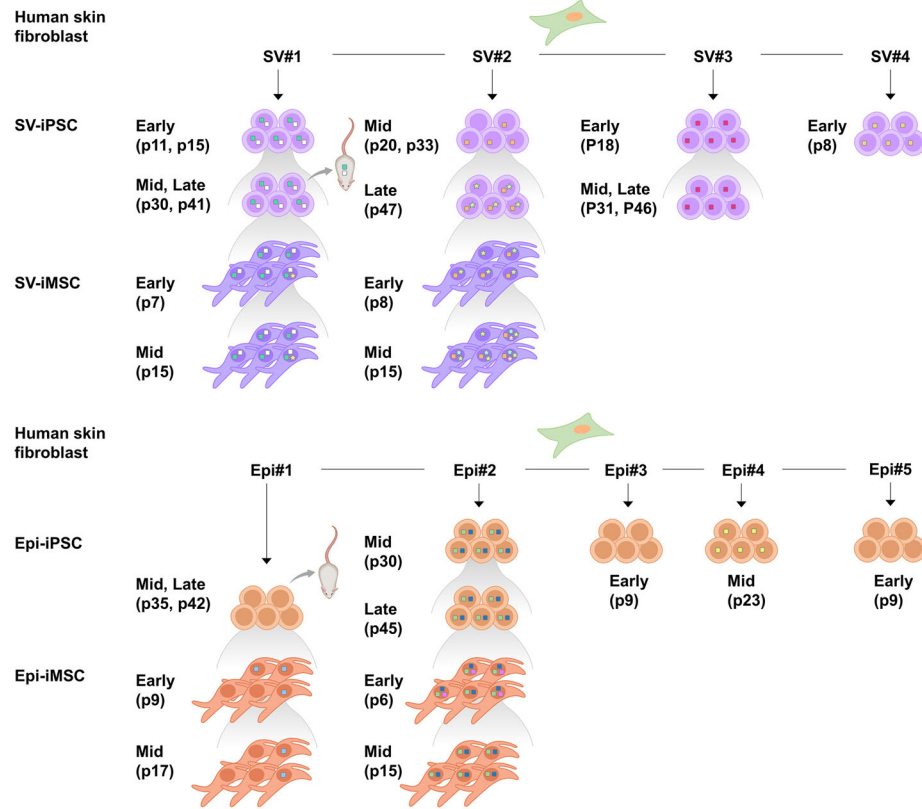
pronounced in late-passage fibroblasts, SV-iPS cells, Epi-iPS cells, SV-iMS cells and Epi-iMS cells compared with early passage cells, leading to increased genomic instability and associated aberrations. Notably, γ H2AX levels were not significantly affected by different reprogramming methods such as non-integrating SV and Epi methods (Supplementary Fig. 4c,d), suggesting that the replication stress levels were similar in iPS cells regardless of the reprogramming method used.

Genomic instability

Genomic stability was evaluated in four SV-iPS cells and five Epi-iPS cells during processing. Additionally, two iMS cell lines differentiated from each of the two iPS cell lines were included

along with their subsequent passages. Of the nine iPS cell lines, six harbored aberrant clones carrying one or two CNAs that were not detected in fibroblasts. All four SV-iPS cells and two of the five Epi-iPS cells exhibited CNAs, which occurred immediately after reprogramming and persisted during subsequent passaging, teratoma formation and iMS cell differentiation (Fig. 4a). Consequently, all four cell lines that differentiated into iMS cells acquired additional CNAs or SNVs. SNVs have only been developed in cell lines derived from SV-iPS cells. All CNAs (Supplementary Table 3) and SNVs were unique and non-recurrent (Fig. 4b).

In SV-iPS cell 1, two CNAs developed after reprogramming and were present in iPS cell passaging (p11–41), early and late-passage iMS cells, and teratoma tissues. The first CNA was 1.27 MB loss in

a**b**

		Genomic alteration	iPSC reprogramming	iPSC passaging	iMSC differentiation	iMSC passaging
SV	iPSC#1	arr[GRCh37] 3q26.31(175356150_175670285) (14 Genes)	●			
	iPSC#1	arr[GRCh37] 7q21.11(77809501_79078925) (15 Genes)	○			
	iPSC#2	arr[GRCh37] 2q21.3q22.1(136610400_137492757) (14 Genes)	●			
	iPSC#3	arr[GRCh37] 10q21.1(53887679_54013793) (12 Genes)	●			
	iPSC#4	arr[GRCh37] 3p22.1(42001363_42378111) (27 Genes)	●			
	iPSC#2	★ <i>TP53</i> c.632C>T (p.Thr211Ile)		■		
	iMSC#1	★ <i>ARID1B</i> c.3092A>T (p.Asp103Val)			■	
	iMSC#2	★ <i>TP53</i> c.745A>T (p.Arg249Trp)				■
	iMSC#2	★ <i>DDX3X</i> c.764A>G (p.Lys255Arg)				■
	iPSC#2	arr[GRCh37] 1p36.33(1482736_1664221) (45 Genes)	○			
Epi	iPSC#2	arr[GRCh37] 3q12.2(100445406_100802027) (7 Genes)	●			
	iPSC#4	arr[GRCh37] 8q22.2(99033353_100013229) (14 Genes)	●			
	iMSC#1	8 Whole chromosome (843 Genes)			●	
	iMSC#2	arr[GRCh37] 3p14.21(59596931_65725694) (7 Genes)			●	

●: CNA gain
○: CNA loss
■: SNV

Fig. 4 The genomic alterations in iPSC cells and iMSC cells through reprogramming, differentiation and passaging. **a**, Nine iPSC cells were produced using two integration-free methods: SV (top, SV-iPSC cell) and episomal vectors (bottom, Epi-iPSC cell). Two iMSC cell lines differentiated from each iPSC cell lines are depicted, including their further passages. In vivo genomic stability was assessed using teratomas, symbolized by a mouse. **b**, Reprogramming-induced CNAs were found in all SV-iPSC cells and two Epi-iPSC cells. All differentiated iMSC cell lines were found to carry exhibited CNA or SNVs. Notably, the all detected genomic aberrations were distinct and showed no recurring pattern. Each alteration was validated using independent methodologies.

chromosome 7q21.11, with a CNA fraction of 0.85–0.98, and the second CNA was a 0.31 MB gain in chromosome 3q26.31, with a CNA fraction of 0.52–0.72. Additionally, a novel SNV in the *ARID1B* gene, identified as Q1031L, emerged in a very small fraction (0.53%) during differentiation. This variant became enriched, reaching 4% in late passages (p15), and was predicted to impact splicing. SV-iPS cell 2 harbored a 0.88-MB-sized gain in chromosome 2q21.3–22.1, which was retained throughout the passages (p20–47) and differentiated into iMS cells. In addition, *TP53* mutation (T211I) appeared in the late-passage iPS cell (p47) and persisted during iMS cell differentiation with a significant allelic fraction of 0.33–0.47. Furthermore, two additional SNVs were found in *TP53* (R249W) and *DDX3X* (K255R) cells in the later passage iMS cell (p15), with small allelic fractions of 0.14 and 0.27, respectively. SV-iPS cell 3 exhibited reprogramming-induced CNAs, including a 0.13 MB gain on chromosome 10q21.1, whereas SV-iPS cell 4 showed a 0.38 MB gain on chromosome 3p22.1.

Epi-iPS cell 1 cells did not exhibit any genomic aberrations during reprogramming and passaging (p35–42) as well in teratoma tissues. After iMS cell differentiation, trisomy 8 emerged and persisted until late-passage p17. Epi-iPS cell 2 harbored two CNAs that remained throughout passaging (p30–45) and differentiated into iMS cells (p6–15). The first CNA was 0.18 MB loss in chromosome 1p36.3, with a CNA fraction of 0.81–0.92, and the second CNA was a 0.36 MB gain in chromosome 3q12.2, with a CNA fraction of 0.45–0.60. In addition, a 0.9 MB gain in 3p14.21 was acquired in the late-passage iPS cell (p45) with a significant burden (0.40–0.50), and this was retained in the iMS cells. Epi-iPS cell 4 exhibited a 1 MB gain on chromosome 8q22.2 with a CNA fraction of 0.61 at a moderate passage (p23), whereas Epi-iPS cells 3 and 5 did not show any genomic aberrations.

In the analysis of the original fibroblast line CRL-2097 across passages 5, 15 and 30, no significant CNAs or SNVs were observed, confirming the impact of reprogramming and differentiation on genomic stability (data not shown).

Changes in gene expression by iPS cell reprogramming methods

The expression levels of 25 genes in the CIN25 signature were evaluated in both mid- and late-passage iPS cells. As presented in Supplementary Table 4, SV-iPS cells (p20 versus p41) exhibited significantly upregulated expression in 24 out of 25 genes, while Epi-iPS cells (p35 versus p42) showed upregulation in 2 out of 25 genes. Downregulated expression was observed in 1 out of 25 genes for SV-iPS cells and in 7 out of 25 genes for Epi-iPS cells. GSEA analysis was conducted to investigate differences in signaling hallmark and Kyoto Encyclopedia of Genes and Genomes pathways (Supplementary Table 5). Supplementary Fig. 5 highlights significantly enriched pathways, including MYC targets, DNA repair, G2M checkpoint, p53 and cancer-related pathways in SV-iPS cells, while Epi-iPS cells showed enrichment in a few pathways including hypoxia and glycolysis.

DISCUSSION

Genetic instability is a significant concern in cell therapy as it is linked to cellular function and/or tumorigenesis. In MS cells, genetic instability typically results in cellular senescence, which is associated with a decrease in the therapeutic efficacy of the cells^{8,19}. However, in iPS cells, various genomic aberrations, including CNAs, SNVs and structural variations, have been observed^{20,21}. Evidence suggests that enhanced cell culture not only leads to prolonged expression of transcription factors, such as c-Myc, but also to the inactivation of *TP53*, and these factors may play a significant role in tumorigenesis. Although it remains unclear whether these genomic aberrations are actual risk factors for adverse events, their presence of genomic aberrations has

raised safety concerns²². iPS cells have become increasingly attractive for regenerative medical applications. However, concerns about their genomic instability and carcinogenic potential have limited their clinical use. To address these concerns, recent advancements in iPS cell technology have employed several integration-free methods^{23,24}. These methods aim to minimize the risk of genomic instability and carcinogenesis associated with iPS cell use²⁵.

In this study, we successfully generated iPS cells using two integration-free methods: SV and episomal vectors. Subsequently, we induced differentiation of these cells into iMS cells. We confirmed the principal characteristics of both iPS cells and iMS cells, maintaining genetic parentality using STR analysis. However, a comprehensive genomic evaluation revealed various genomic aberrations.

γH2AX staining indicated higher replication stress and DNA damage in iPS cells, regardless of the reprogramming method used. Notably, all SV-iPS cell lines exhibited CNAs during the reprogramming process, whereas only 40% of Epi-iPS cells showed such alterations. Additionally, SNVs were observed in SV-iPS cells and SV-iMS cells, but not in Epi-iPS cell and Epi-iMS cell lines. Gene expression analysis revealed that the majority of genes in the CIN25 signature were upregulated in late-passage SV-iPS cells compared with mid passage, suggesting increased chromosomal instability with prolonged passaging. In contrast, Epi-iPS cells showed upregulation in only 2 out of 25 genes, indicating a more stable gene expression profile. Similarly, GSEA revealed that in SV-iPS cells, significant pathways related to DNA repair, p53 and cancer were enriched during passaging, while these changes were less pronounced in Epi-iPS cells. This further supports the notion that Epi-iPS cells maintain better genomic stability than SV-iPS cells. Several studies have reported small genomic alterations in iPS cell lines, including CNAs and SNVs, which may reflect the mutagenic effects of the reprogramming process itself^{26–28}. Studies have demonstrated that different reprogramming methods, whether integrating or non-integrating, have varied impacts on replication stress and genomic integrity^{29,30}. Non-integrating methods, including SV-, Epi-, mRNA- and protein-based methods, mitigate the risks associated with direct genetic modification, making them safer for clinical applications and research^{30–32}. However, little is known about which of these non-integrating methods is superior in preserving genomic stability. Our findings highlight the relative stability of the Epi-based method. Further comparative studies between iPS cells generated by various non-integrating and integrating reprogramming methods are crucial for understanding and mitigating risks, thereby promoting safer and more effective clinical applications.

The detected genomic aberrations were individualized; therefore, we could not identify common changes. Analytical technologies, SNP arrays and NGS with sufficient depth are required to identify genomic aberrations^{33,34}. Most genetic aberrations were interstitial duplications detected by the SNP array, which were primarily acquired during the reprogramming process. These amplified regions included genes with critical functions: *MCM6* and *PTPRG* in cellular replication; *DARS*, *RPL30* and *POP1* in protein synthesis; and *HRP512* and *STK3* in maintaining cellular homeostasis. We also observed interstitial losses in *CDK11A*, *CDK11B* and *SSU72* genes, which encode enzymes vital for cell division. During iMS cell differentiation, a clone with trisomy 8 developed, leading to the amplification of the *MYC* oncogene^{35–37}. This clone rapidly supplanted half of the iMS cell population, indicating high replicative capacity. SNVs were detected in *ARID1B*, *TP53* and *DDX3X* genes via NGS. The *ARID1B* gene functions to regulate gene expression through chromatin remodeling and is associated with several developmental health conditions and cancers^{38–40}. The *DDX3X* gene encodes a DEAD-box RNA helicase that plays a crucial role in cell cycling, apoptosis and tumorigenesis. Notably, two *TP53* mutations were observed, making it the only well-known

tumor suppressor gene for which mutations have been detected in multiple iPS cell lines⁴¹. The late-occurring *TP53* mutation is a well-defined oncogenic variant (COSM43629) that is accompanied by a *DDX3X* mutation, indicating a sudden increase in genomic instability.

This study had several limitations. First, the reprogramming process was conducted using a single set of purchased human fibroblasts, which limited our ability to analyze potential genomic aberrations across a broader range of donor-specific differences. Second, we did not confirm the functional consequences of the detected genetic aberrations. Third, our data revealed a high incidence of genomic aberrations, especially SNVs, in cell lines generated using the SV method. However, further verification through additional studies is required.

Our study suggests that iPS cells are prone to genomic aberrations throughout all processes, including differentiation into iMS cells. iPS cells generated using the SV method exhibit greater genomic instability compared with those generated with episomal vectors. SV-iPS cells displayed a higher frequency of CNAs and SNVs, along with increased expression of chromosomal instability genes, indicating a higher risk of genomic aberrations during extended culture. Notably, CNAs are frequently associated with replication-related genes. The identification of *TP53* mutations underscores the vulnerability of the gene and highlights the need for careful scrutiny when preparing iPS cells and derived cell lines.

REFERENCES

- Bianco, P. et al. The meaning, the sense and the significance: translating the science of mesenchymal stem cells into medicine. *Nat. Med.* **19**, 35–42 (2013).
- Sharma, R. R., Pollock, K., Hubel, A. & McKenna, D. Mesenchymal stem or stromal cells: a review of clinical applications and manufacturing practices. *Transfusion* **54**, 1418–1437 (2014).
- Sabapathy, V. & Kumar, S. hiPSC-derived iMSCs: nextgen MSCs as an advanced therapeutically active cell resource for regenerative medicine. *J. Cell Mol. Med.* **20**, 1571–1588 (2016).
- Xu, M., Shaw, G., Murphy, M. & Barry, F. Induced pluripotent stem cell-derived mesenchymal stromal cells are functionally and genetically different from bone marrow-derived mesenchymal stromal cells. *Stem Cells* **37**, 754–7653 (2019).
- Zhang, J. et al. Induced pluripotent stem cell-derived mesenchymal stem cells hold lower heterogeneity and great promise in biological research and clinical applications. *Front. Cell Dev. Biol.* **9**, 716907 (2021).
- Chakradhar, S. An eye to the future: researchers debate best path for stem cell-derived therapies. *Nat. Med.* **22**, 116–119 (2016).
- Kim, M. et al. Passage-dependent accumulation of somatic mutations in mesenchymal stromal cells during in vitro culture revealed by whole genome sequencing. *Sci. Rep.* **7**, 14508 (2017).
- Kim, J. et al. Ubiquitin C decrement plays a pivotal role in replicative senescence of bone marrow mesenchymal stromal cells. *Cell Death Dis.* **9**, 139 (2018).
- Son, M. Y. et al. Generation and characterization of integration-free induced pluripotent stem cells from patients with autoimmune disease. *Exp. Mol. Med.* **48**, e232 (2016).
- Jang, Y. et al. Development of immunocompatible pluripotent stem cells via CRISPR-based human leukocyte antigen engineering. *Exp. Mol. Med.* **51**, 1–11 (2019).
- Na, D. H. et al. Generation of a human induced pluripotent stem cell line (CMC001-A) from a patient with karyomegalic interstitial nephritis with homozygous frameshift deletion mutation c.1985_1994del10 of the *FANCD2/FANCI*-Associated Nuclease 1 gene. *Stem Cell Res.* **46**, 101876 (2020).
- Choi, H. et al. Common and different alterations of bone marrow mesenchymal stromal cells in myelodysplastic syndrome and multiple myeloma. *Cell Prolif.* **53**, e12819 (2020).
- Carter, S. L., Eklund, A. C., Kohane, I. S., Harris, L. N. & Szallasi, Z. A signature of chromosomal instability inferred from gene expression profiles predicts clinical outcome in multiple human cancers. *Nat. Genet.* **38**, 1043–1048 (2006).
- Dominici, M. et al. Minimal criteria for defining multipotent mesenchymal stromal cells. The International Society for Cellular Therapy position statement. *Cytotherapy* **8**, 315–317 (2006).
- Lv, F.-J., Tuan, R. S., Cheung, K. M. & Leung, V. Y. Concise review: the surface markers and identity of human mesenchymal stem cells. *Stem Cells* **32**, 1408–1419 (2014).
- Pittenger, M. F. et al. Mesenchymal stem cell perspective: cell biology to clinical progress. *npj Regen. Med.* **4**, 22 (2019).
- Petrenko, Y. et al. A comparative analysis of multipotent mesenchymal stromal cells derived from different sources, with a focus on neuroregenerative potential. *Sci. Rep.* **10**, 4290 (2020).
- Vallabhaneni, H. et al. High basal levels of γH2AX in human induced pluripotent stem cells are linked to replication-associated DNA damage and repair. *Stem Cells* **36**, 1501–1513 (2018).
- Burkhalter, M. D., Rudolph, K. L. & Sperka, T. Genome instability of ageing stem cells-Induction and defence mechanisms. *Ageing Res. Rev.* **23**, 29–36 (2015).
- Martins-Taylor, K. & Xu, R. H. Concise review: genomic stability of human induced pluripotent stem cells. *Stem Cells* **30**, 22–27 (2012).
- Oliveira, P. H., da Silva, C. L. & Cabral, J. M. Concise review: genomic instability in human stem cells: current status and future challenges. *Stem Cells* **32**, 2824–2832 (2014).
- Yoshihara, M. & Murakawa, Y. in *Current Topics in iPSCs Technology* Vol. 17 (ed. Birbrair, A.) 147–175 (Academic, 2022).
- Yu, J. et al. Human induced pluripotent stem cells free of vector and transgene sequences. *Science* **324**, 797–801 (2009).
- Okita, K. et al. A more efficient method to generate integration-free human iPS cells. *Nat. Methods* **8**, 409–412 (2011).
- Thompson, O. et al. Low rates of mutation in clinical grade human pluripotent stem cells under different culture conditions. *Nat. Commun.* **11**, 1528 (2020).
- Gore, A. et al. Somatic coding mutations in human induced pluripotent stem cells. *Nature* **471**, 63–67 (2011).
- Laurent, L. C. et al. Dynamic changes in the copy number of pluripotency and cell proliferation genes in human ESCs and iPSCs during reprogramming and time in culture. *Cell Stem Cell* **8**, 106–118 (2011).
- Schlaeger, T. M. et al. A comparison of non-integrating reprogramming methods. *Nat. Biotechnol.* **33**, 58–63 (2015).
- González, F., Boué, S. & Izpisua Belmonte, J. C. Methods for making induced pluripotent stem cells: reprogramming à la carte. *Nat. Rev. Genet.* **12**, 231–242 (2011).
- Bhutani, K. et al. Whole-genome mutational burden analysis of three pluripotency induction methods. *Nat. Commun.* **7**, 10536 (2016).
- Steinle, H. et al. Generation of iPSCs by nonintegrative RNA-based reprogramming techniques: benefits of self-replicating RNA versus synthetic mRNA. *Stem Cells Int.* **2019**, 7641767 (2019).
- Park, H. et al. Increased genomic integrity of an improved protein-based mouse induced pluripotent stem cell method compared with current viral-induced strategies. *Stem Cells Transl. Med.* **3**, 599–609 (2014).
- Yoshihara, M., Hayashizaki, Y. & Murakawa, Y. Genomic instability of iPSCs: challenges towards their clinical applications. *Stem Cell Rev. Rep.* **13**, 7–16 (2017).
- Jo, H. Y. et al. Development of genetic quality tests for good manufacturing practice-compliant induced pluripotent stem cells and their derivatives. *Sci. Rep.* **10**, 3939 (2020).
- Liu, P. et al. Passage number is a major contributor to genomic structural variations in mouse iPSCs. *Stem Cells* **32**, 2657–2667 (2014).
- Taapken, S. M. et al. Karyotypic abnormalities in human induced pluripotent stem cells and embryonic stem cells. *Nat. Biotechnol.* **29**, 313–314 (2011).
- Nikitina, V. et al. Clonal chromosomal and genomic instability during human multipotent mesenchymal stromal cells long-term culture. *PLoS ONE* **13**, e0192445 (2018).
- Hoyer, J. et al. Haploinsufficiency of ARID1B, a member of the SWI/SNF-a chromatin-remodeling complex, is a frequent cause of intellectual disability. *Am. J. Hum. Genet.* **90**, 565–572 (2012).
- Khursheed, M. et al. ARID1B, a member of the human SWI/SNF chromatin remodeling complex, exhibits tumour-suppressor activities in pancreatic cancer cell lines. *Br. J. Cancer* **108**, 2056–2062 (2013).
- Vasileiou, G. et al. Chromatin-remodeling-factor ARID1B represses Wnt/β-catenin signaling. *Am. J. Hum. Genet.* **97**, 445–456 (2015).
- Merkle, F. T. et al. Human pluripotent stem cells recurrently acquire and expand dominant negative P53 mutations. *Nature* **545**, 229–233 (2017).

ACKNOWLEDGEMENTS

This research was funded by Ministry of Food and Drug Safety (grant number 22202MFD5127), supported by the Korean Fund for Regenerative Medicine (23A0106L1), the KRIBB research initiative program (KGM1232511) and the National Research Foundation of Korea (NRF) (grant RS-2023-00272798).

COMPETING INTERESTS

The authors declare no competing interests.

ADDITIONAL INFORMATION

Supplementary information The online version contains supplementary material available at <https://doi.org/10.1038/s12276-025-01439-8>.

Correspondence and requests for materials should be addressed to Yee Sook Cho or Myungshin Kim.

Reprints and permission information is available at <http://www.nature.com/reprints>

Publisher's note Springer Nature remains neutral with regard to jurisdictional claims in published maps and institutional affiliations.



Open Access This article is licensed under a Creative Commons Attribution 4.0 International License, which permits use, sharing, adaptation, distribution and reproduction in any medium or format, as long as you give appropriate credit to the original author(s) and the source, provide a link to the Creative Commons licence, and indicate if changes were made. The images or other third party material in this article are included in the article's Creative Commons licence, unless indicated otherwise in a credit line to the material. If material is not included in the article's Creative Commons licence and your intended use is not permitted by statutory regulation or exceeds the permitted use, you will need to obtain permission directly from the copyright holder. To view a copy of this licence, visit <http://creativecommons.org/licenses/by/4.0/>.

© The Author(s) 2025